Nouroze Gul, Sadia Ata, Ismat Bibi*, Ijaz-ul-Mohsin, Muhammad Azam, Abubaker Shahid, Norah Alwadai, Nasir Masood and Munawar Iqbal

Size controlled synthesis of silver nanoparticles: a comparison of modified Turkevich and BRUST methods

https://doi.org/10.1515/zpch-2022-0009
Received January 13, 2022; accepted May 20, 2022; published online June 20, 2022

Abstract: In the present investigation, silver nanoparticles were synthesized and a comparative analysis was performed of modified Turkevich and BRUST methods. Silver nitrate precursor was reduced by trisodium citrate dihydrate and ascorbic acid was used as a surfactant. Based on Turkevich and BRUST methods, the process variables, i.e., temperature, reducing agent concentration, stirring speed, mode of injecting reducing agent/precursor to large excess volume of either precursor/reducing agent were studied. The size of the particles was preliminarily ascertained by DLS studies and it was found that modified BRUST method yielded silver nanoparticles with average particle size of 25 nm, while modified Turkevich method furnished nanoparticles with average particle size of 15 nm. The silver nanoparticles were characterized by employing the UV/visible, Zeta sizer, scanning electron microscopy (SEM) and energy dispersive microscopy (EDX) techniques. Results revealed that the silver nanoparticles size can be controlled by optimizing the conditions of modified Turkevich and BRUST methods.

***Corresponding author: Ismat Bibi**, Institute of Chemistry, The Islamia University of Bahawalpur, Bahawalpur, Pakistan, E-mail: drismat@iub.edu.pk
Nouroze Gul, School of Chemistry, University of the Punjab, Lahore, Pakistan; and Institute of Nuclear Medicine and Oncology, Lahore, Pakistan
Sadia Ata and Muhammad Azam, School of Chemistry, University of the Punjab, Lahore, Pakistan
Ijaz-ul-Mohsin, Institute for Applied Materials–Applied Materials Physics (IAM-AWP), Karlsruhe Institute of Technology, Karlsruhe, Germany
Abubaker Shahid, Institute of Nuclear Medicine and Oncology, Lahore, Pakistan
Norah Alwadai, Department of Physics, College of Sciences, Princess Nourah bint Abdulrahman University, P.O. Box 84428, Riyadh 11671, Saudi Arabia
Nasir Masood, Department of Environmental Sciences, COMSATS University Islamabad, Vehari Campus, Punjab, Pakistan
Munawar Iqbal, Department of Chemistry, Division of Science and Technology, University of Education, Lahore, Pakistan

Keywords: silver nanoparticles; size control; size distribution; surface morphology; UV/visible.

1 Introduction

The nanotechnology is one of promising substitute to traditional chemotherapy due to numerous benefits provided by nanocarriers with remarkable drug loading capacity, longer half-life, low toxicity and targeted drug delivery. Nanoparticles have got impetus in the current era and being used in several fields, i.e., nanoelectronics, aeronautical engineering, environmental safety, consumer goods and medical healthcare [1, 2]. Metal nanocarriers have biological applications owing to their drug carrying efficiency and potential diagnostic efficiency, which make them a theragnostic agents [3]. Recently, the unique properties of nanomaterials, i.e., passive, active transport and physical targeting have stimulated efforts in improving biomedical applications [4–8]. The intrinsic cytotoxicity of silver NPs has authenticated their utilization as antibacterial and anticancer agents in the fields of biomedicine in healthcare industry. The value of surface charge determine the cytotoxicity of Ag NPs [3, 9]. The positively charged silver NPs are more suitable to be retained longer on the tissues/blood vessel luminal side, which is a key route to administer anticancer agents. The inherent cellular toxicity of silver NPs was employed to combat different forms of cancer cells, i.e., hepatocellular cancer, lungs and breast cancer and cervical carcinoma [10–14]. A number of findings have revealed that the silver NPs were more effective in the biological systems. Silver NPs have been studied and found as efficient agents to combat angiogenesis and cancer issue [3]. Silver NPs are efficient anti-proliferative agents against cancer cells because they are capable to damage DNA that causes chromosomal breakage, genomic instability thus disrupts calcium (Ca^{2+}) homeostasis and thus apoptosis was induced that causes cytoskeletal instability. The damaged cytoskeletal prevent the cellular division and cell cycle and result in blocking the proliferation of cancer cells [15]. The small nanoparticles demonstrate enhanced permeation in tumor cells in consequence of enhanced permeability and retention (EPR) effects which leads to accumulation of nanosized contrast agents in the tumor cells [16]. The size distribution of nanoparticles plays a pivotal role for the imaging studies of tumor. The nanoparticles size impacts the biodistribution profile, blood circulation time, cell penetration thus causing tumor penetration and targeting [17]. The excretion of nanoparticles is size dependent manner and the size of renal filtration pore is found to be on average in the order of 10 nm [18]. Hence, the particles as small as 10 nm or less are quickly excreted by renal system [19]. Contrarily, the bigger NPs with more than 100 nm size show higher uptake in the organs with mononuclear phagocytic system (MPS), i.e., accumulate in liver, spleen, lymph nodes and lungs [20]. The size of silver nanoparticles intended for biomedical

applications was attributed high interest, since it was observed that smaller the Ag NPs, more the cytotoxic effect and vice versa [21]. The small nanoparticles less than 15 nm were more cytotoxic as compared to particles with larger size. Thus, 10 nm Ag NPs were cytotoxic for normal cells of human lung epithelium, irrespective the type of surface coating (PVP or Citrate) [22]. It was further established by a study conducted on four cell lines that the silver NPs of 5 nm express more cytotoxicity as compared with the same particles in the sizes of 20 nm and 50 nm [23]. The nanoparticles in the size range of 10–60 nm consistently express higher cellular uptake [17]. It was further evaluated that the rods and discs shaped silver nanoparticles exhibit more appropriate blood circulation properties as compared with spherical shaped, however, the spherical Ag NPs reveal enhanced cellular permeation probably due to more appropriate binding properties to the target sites [24] and possess more thermodynamic stability [25]. It was further emphasized that the shape of the Silver NPs is a very significant factor to evaluate the possible interactions within body cells, while the spherical form was recommended for biomedical applications due to a reduced *in-vivo* cellular toxicity [26].

It is evident that the nanoparticles with ultrafine size, desired shape and size distribution have gained much attention due their ideal properties. The metal nanoparticles can be synthesized with desired features by altering the fabrication protocols, reducing and stabilizing agents [3, 27–30]. The careful consideration of these parameters aid to attain nanoparticles with desired physical and chemical attributes. Commonly, metallic NPs can be synthesized either by physical, biological and chemical routes. However, chemical reduction method is the most commonly used method due to its simplicity and process control. This method also enables variation in the molar concentration of the reducing agent/precursor, dispersant and feed rate of reducing agent/precursor in order to produce silver nanoparticles with controlled particle sizes, shapes and particle size distribution. The selection of a suitable reducing agent is also an important factor, as the size, shape and particle size distribution are also depending on the nature of the reducing agent. The reducing agent causes the reduction of precursor metal ions and reduction of metal ions needs the reducing agent reactivity to the redox potential of the metal. During the nanoparticles synthesis, the size of nanoparticles depends upon the rate of reaction. In case, the reaction rate is too fast, rapid formation of a large number of metal nuclei take place and result in smaller particles. On the other hand, slower reaction rate causes agglomeration of smaller particles to bigger ones. Moreover, the choice of the surfactant is very important as it decides not only the size and shape of nanoparticles, but it also impacts the reactivity, solubility, stability, dispersity of nanoparticles during preparation [31]. Previous studies regarding synthesis of metal nanoparticles utilizing strong reducing agents, i.e., $NaBH_4$ have shown the fabrication of small monodispersed colloidal formulations, but formation of larger aggregates of silver NPs was

difficult to control. The use of citrate, a weaker reducing agent, led to slower rate of reduction which leads to control the size and shape of NPs [32].

Based on aforementioned facts, size-controlled synthesis of silver nanoparticles was performed based on modified Turkevich and BRUST methods. The prepared silver nanoparticles were characterized by employing the UV/visible, Zeta sizer and scanning electron microscopy (SEM) and energy dispersive microscopy (EDX) techniques. The conditions such as temperature, reducing agent concentration, stirring speed, mode of injecting reducing agent/precursor to large excess volume of either precursor/reducing agent were also studied to control the size of the silver nanoparticles.

2 Material and methods

2.1 Chemical and reagents

Analytical grade, $AgNO_3$ (Sigma-Aldrich Germany), trisodium citrate dehydrate ($C_6H_5O_7Na_3.2H_2O$, Sigma-Aldrich, Germany), ascorbic acid ($C_6H_8O_6$, Merck, Germany) and ultrapure water (Millipore system) were used. The UV/VIS Spectrophotometer (Hitachi U-2910), Zetasizer (Malvern Nano series ZS 90) and SEM (Hitachi SX-650) techniques were employed for the characterization of the prepared samples.

2.2 Synthesis protocols

In the synthesis procedure, the reducing agent trisodium citrate dihydrate ($C_6H_5O_7Na_3.2H_2O$) and surfactant ascorbic acid ($C_6H_8O_6$) mixture was added to the large excess of $AgNO_3$ salt solution, $AgNO_3$ precursor was added to the larger volume of reducing agent and surfactant mixture solution. Various reaction conditions were designed by varying the reaction conditions and their effect on the particle size was studied, i.e., variable concentration of reducing agent, magnetic stirring speed and feed rate of reducing agent/precursor.

2.2.1 BRUST method: In the modified BRUST method, 100 ml of 1 mmol $AgNO_3$ solution was heated and then (with continuous stirring) 20 ml mixture solution comprising of 1 mmol ascorbic acid and variable concentrations of trisodium citrate ranging from 6 mmol to 9 mmol was added. The final ratio of $AgNO_3$:$C_6H_5O_7Na_3.2H_2O$ was as, 1:1.2 for 6 mM citrate, 1:1.4 for 7 mM citrate, 1:1.6 for 8 mM citrate, 1:1.8 for 9 mM citrate. The ratio of $AgNO_3$: $C_6H_8O_6$ is 1:0.2 which is constant for all the preparations. The contents were stirred for 10 min to complete the formulation process. The suspension was then cooled for centrifugal separation at 13500 rpm for 20 min for further characterization. In this method the small, monodispersed particles were attained by optimizing the reaction conditions. In optimized protocol, 100 mL 1 mmol silver nitrate solution was heated at 75 °C and stirring was kept at 1400 rpm. Then, 20 mL reducing agent and surfactant mixture solution (1 mM ascorbic acid and 9 mM citric acid) was added. Then stirring was continued for

10 min. The change in solution color takes place from pale yellow to brownish green indicating the formation of silver nanoparticles. This was named as sample A.

2.2.2 Turkevich method: In the modified Turkevich method, the reducing agent and surfactant mixture was taken in flask and heated at 75 °C and magnetic stirring was maintained at 1400 rpm prior to addition of silver salt solution. Then, 2 ml (50 mM) $AgNO_3$ was added. The particle size was determined varying the reaction conditions, i.e., temperature, stirring speed, mode of injection of precursor to the reducing agent and variable concentration of $C_6H_5O_7Na_3.2H_2O$. In the optimized protocol, 100 mL mixture solution containing 4 mM $C_6H_5O_7Na_3.2H_2O$ and 0.5 mM $C_6H_8O_6$ was heated to 75 °C and with continuous stirring at 1400 rpm, 2 mL (50 mM) silver nitrate solution was injected immediately. The solution color was changed, first light yellow and finally, reddish brown indicating the formation of silver nanoparticles. The contents were stirred for 10 min, cooled and centrifugal separation was done. This was named as sample B.

2.2.3 Characterization: The synthesis of silver NPs was characterized by UV/VIS analysis, while hydrodynamic size (Zav) and size distribution was measured by Zeta sizer. The morphology of the silver NPs was determined by SEM analysis. The surface charge (Zeta potential) was measured by zeta sizer to determine colloidal suspension stability of NPs.

3 Results and discussion

3.1 UV/vis analysis

Figure 1 demonstrated the UV/vis spectra of silver NPs, which indicate maximum SPR at 407 for 15 nm silver nanoparticles and 430 for 25 nm particles. Silver nanoparticles possess unique optical properties, which are responsible for their strong interaction with specific wavelengths of light [33]. In silver NPs, the close proximity of valance band and conduction band give rise to free movement of electrons, which results in surface plasmon resonance (SPR) absorption band generated due to combined oscillation of Ag NPs free electrons in resonance with the light wave [34, 35]. The absorption band of silver nanoparticle depends upon its size and dielectric of adjacent medium and chemical surroundings [36, 37]. It was reported that Silver NPs of various sizes synthesized by biological method using gallic acid as stabilizer were characterized by this technique [38] and it was proved that spherical silver NPs of 7 nm size exhibited SPR at 410 nm, while the particles of size 29 nm showed absorption maxima at 425 nm. In the same way, the silver NPs of 89 nm exhibited a wider band showing maximum absorbance at 490 nm. It was ascertained that the SPR band width represent the size distribution of nanoparticles.

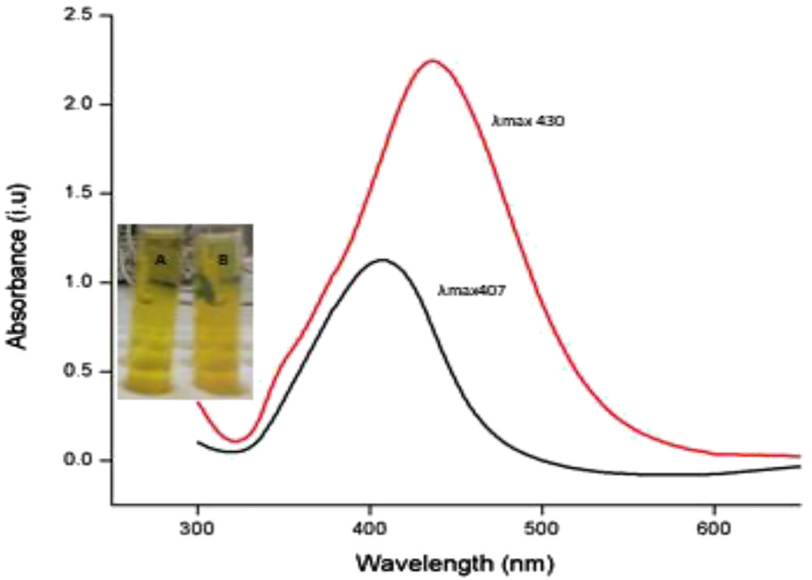

Figure 1: UV/Vis analysis of silver NPs of sample A λ_{max} 430 (modified brust method) and sample B λ_{max} 407 (modified Turkevich method).

3.2 Morphology and composition analysis

The morphology was studied by SEM analysis and response is shown in Figures 2 and 3. The SEM micrographs revealed sample A nanoparticles was spherical in shape and non-uniform size distribution was observed. Moreover, the particles are in close proximity due to the assembly of smaller particles, but in the aggregated assembly the NPs retain their separate identity indicating the stable suspension. The SEM micrograph of sample B, the particles were found to be uniform in size and in spherical shape. The shape of silver NPs is an important parameter to determine the cellular uptake and medical applications because their administration in the body involve low toxicity [26]. The chemical purity of silver NPs dispersion was ensured by energy dispersive X-ray spectroscopy (EDX) used jointly with SEM yielded not only the morphology of silver nanoparticles, but also perform chemical analysis, which revealed the formation of silver nanoparticles (Figures 4 and 5).

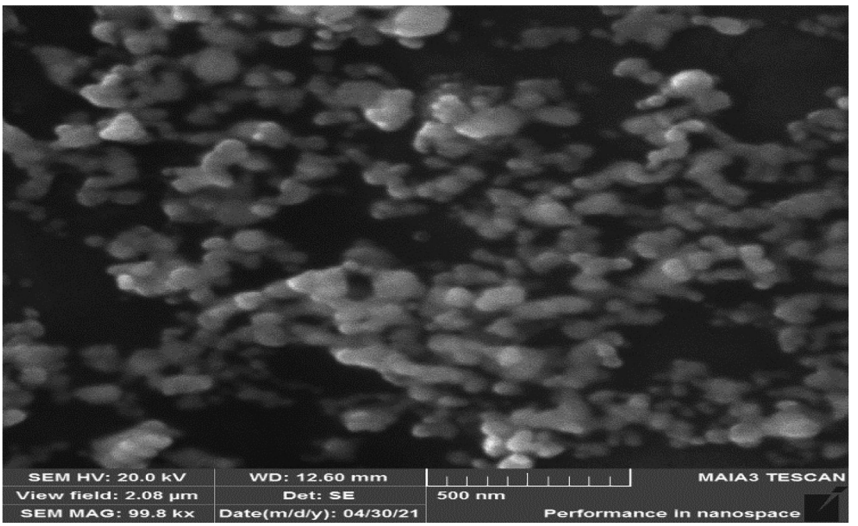

Figure 2: SEM image of silver nanoparticles of sample A (modified BRUST method).

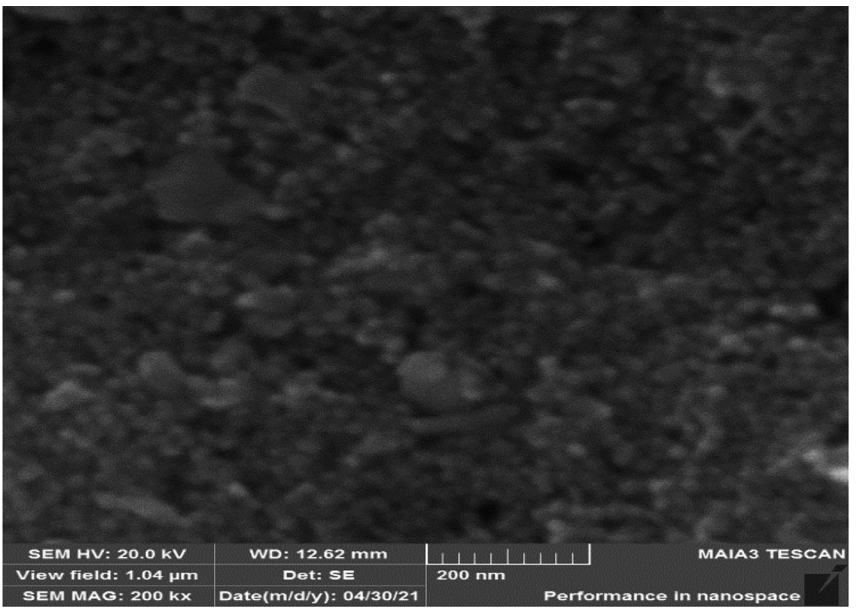

Figure 3: SEM image of silver nanoparticles of sample B (modified Turkevich method).

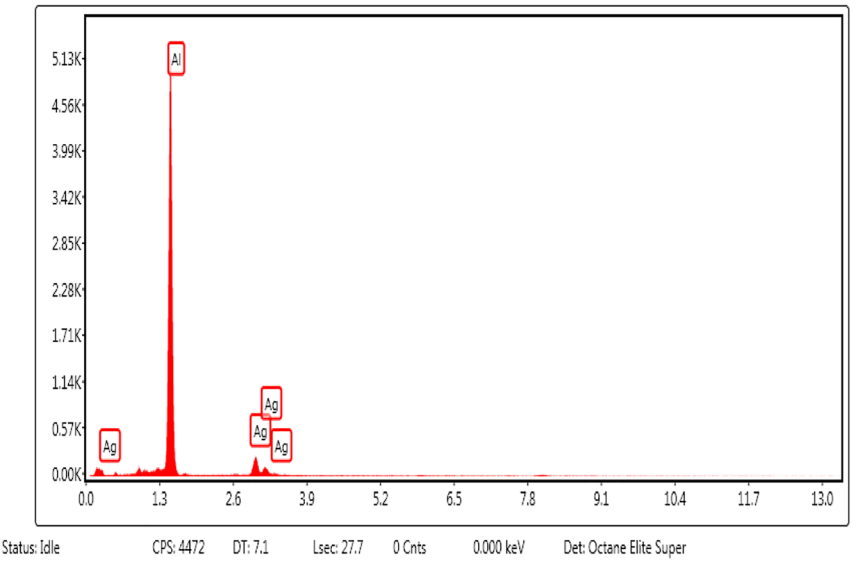

Figure 4: EDX analysis of silver nanoparticles of sample A (modified BRUST method).

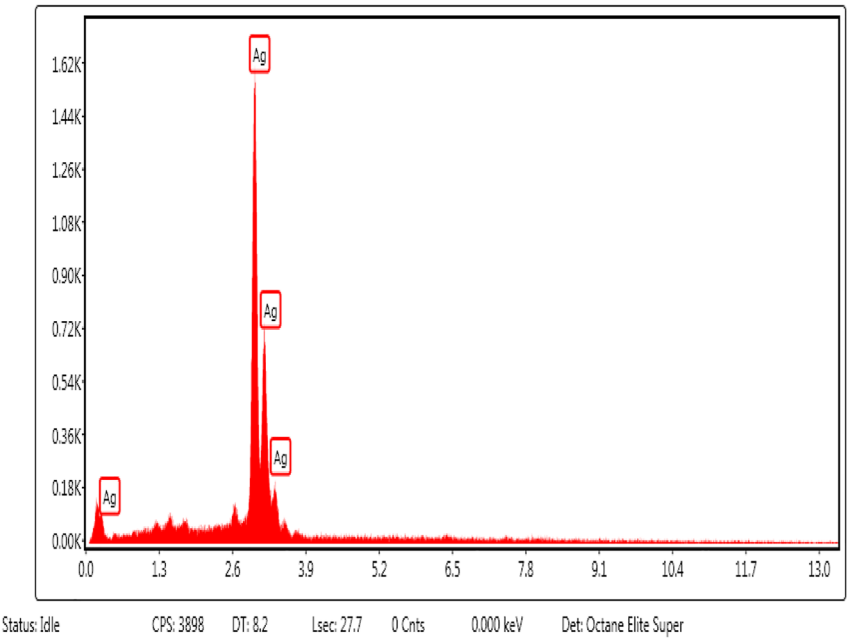

Figure 5: EDX analysis of silver nanoparticles of sample B (modified Turkevich method).

3.3 Surface charge analysis

The zeta potential values of sample A and sample B were measured on zetasizer and found to be −31 mV and −35 mV, respectively. The highly negative or highly positive values of zeta potential indicated the stability of colloidal suspension due to strong repulsion generated by highly positive or highly negative nanoparticles solution that prevents particles aggregation. The NPs with positive surface zeta potential value higher than +20 mV or negative zeta potential value greater than −20 mV are usually thought to be stable as the repulsion between the particles inhibit agglomeration [39]. A number of studies demonstrated stability of nanoparticles as a critically important factor to determine their applications in the field of medicine [40, 41]. Zeta potential values (−31 mV) for sample A and (−35 mV) for sample B noted in the present work represented the stability of the nanoparticles suspension, which is in line with reported studies.

3.4 Ag NPs formation mechanism and size distribution

In the current investigation, silver nanoparticles were synthesized by the reduction process approach. In the beginning of reduction reaction, silver cations (Ag^+) in solution phase were reduced to silver atom (Ag^0). When reduction progress, more silver atoms were generated, which act as nucleation centers and coalescence of metal atoms create metal clusters which are normally stabilized by surfactants, ligands or polymers [42]. The ascorbic acid being surfactant was supposed to prevent agglomeration and thus controlled the size of nanoparticles by being adsorbed on the metal atoms surface. It was reported that the metal atoms (Ag^0) obtained at the start of reduction reaction behave as nucleation centers and their continuous growth with the progress of reaction result in a number of color changes from pale yellow to yellow and then reddish brown or green showing the formation and growth of silver NPs. The reaction for the synthesis of silver NPs is expressed in Eq. (1) [43].

$$4Ag^+ + C_6H_5O_7Na_3 + 2H_2O \rightarrow 4Ag^0 + C_6H_5O_7H_3 + 3Na^+ + H^+ + O_2 \quad (1)$$

The results obtained from various reaction protocols obtained from modified BRUST method and modified Tukevich methods are summarized in Table 1 and 2. In the modified BRUST method, the precursor $AgNO_3$ was first heated and then with constant stirring a mixture solution of $C_6H_5O_7Na_3.2H_2O$ and $C_6H_8O_6$ was added. As the stirring rate of heated precursor was varied, the resulting effect on particle size was measured by zeta sizer and found that increasing the stirring rate increased the Zav from 34 at 400 rpm to 36 at 1000 rpm, while increase in temperature causes a decrease in particle size. When temperature was increased from 60 °C to 70 °C

Table 1: Effect of experimental conditions on size of nanoparticles in a modified BRUST method.

Reaction conditions	Ratio of molar concentration of $AgNO_3$: $C_6H_5O_7Na_3.2H_2O$ (mmol)	Concentration of surfactant/stabilizer $C_6H_8O_6$ (mmol)	Temperature (°C)	Stirring rate (rpm)	Mode of injection of reducing agent	Average hydrodynamic size (Zav) (nm)
Impact of reducing agent concentration	1:1.2	0.2	75	1400	At once	40
	1:1.4	0.2	75	1400	At once	38
	1:1.6	0.2	75	1400	At once	33
	1:1.8	0.2	75	1400	At once	25
Impact of stirring	1:1.6	0.2	70	400	Dropwise	34
	1:1.6	0.2	70	700	Dropwise	35
	1:1.6	0.2	70	1000	Dropwise	36
Impact of temperature	1:1.6	0.2	60	700	Dropwise	49
	1:1.6	0.2	70	700	Dropwise	34
Size optimization conditions (sample A)	1:1.8	0.2	75	1400	At once	25

Table 2: Effect experimental conditions on the size of nanoparticles in a modified Turkevich.

Reaction conditions	$AgNO_3$Conc (mmol)	Molarity of $Na_3C_6H_5O_7.2H_2O$ (mmol)	Concentration of surfactant/stabilizer $C_6H_8O_6$ (mmol)	Temperature (°C)	Stirring rate (rpm)	Mode of Injection of reducing agent	Average Hydrodynamic size (Zav) (nm)
Impact of temperature	2 ml $AgNO_3$ (50 mM)	4	0.5	60	700	Dropwise	33
	2 ml $AgNO_3$ (50 mM)	4	0.5	70	700	Dropwise	31
	2 ml $AgNO_3$ (50 mM)	4	0.5	75	700	Dropwise	28
Impact of stirring rate	2 ml $AgNO_3$ (50 mM)	4	0.5	70	400	Dropwise	27
	2 ml $AgNO_3$ (50 mM)	4	0.5	70	700	Dropwise	28
	2 ml $AgNO_3$ (50 mM)	4	0.5	70	1000	Dropwise	30
Size optimization conditions sample (B)	2 ml $AgNO_3$ (50 mM)	4	0.5	75	1400	At once	15

particle size was decreased from 49 nm to 34 nm. Many investigations have reported the impact of temperature on the size and shape of NPs. Spherical nanoparticles are synthesized at an elevated temperature, while generally the nanotriangle formation takes place at lower temperature [44]. It has been reported that raising temperature between 30 °C and 90 °C enhances the rate of reaction for nanoparticles synthesis [45, 46] and higher temperature also supports the formation of smaller silver nanoparticles [46]. In the same way, when the ratio of $AgNO_3$: $C_6H_5O_7Na_3.2H_2O$ was increased from 1:1.2 to 1:1.8, a consequent decrease in particle size from 40 nm to 25 nm was observed (Figure 6).

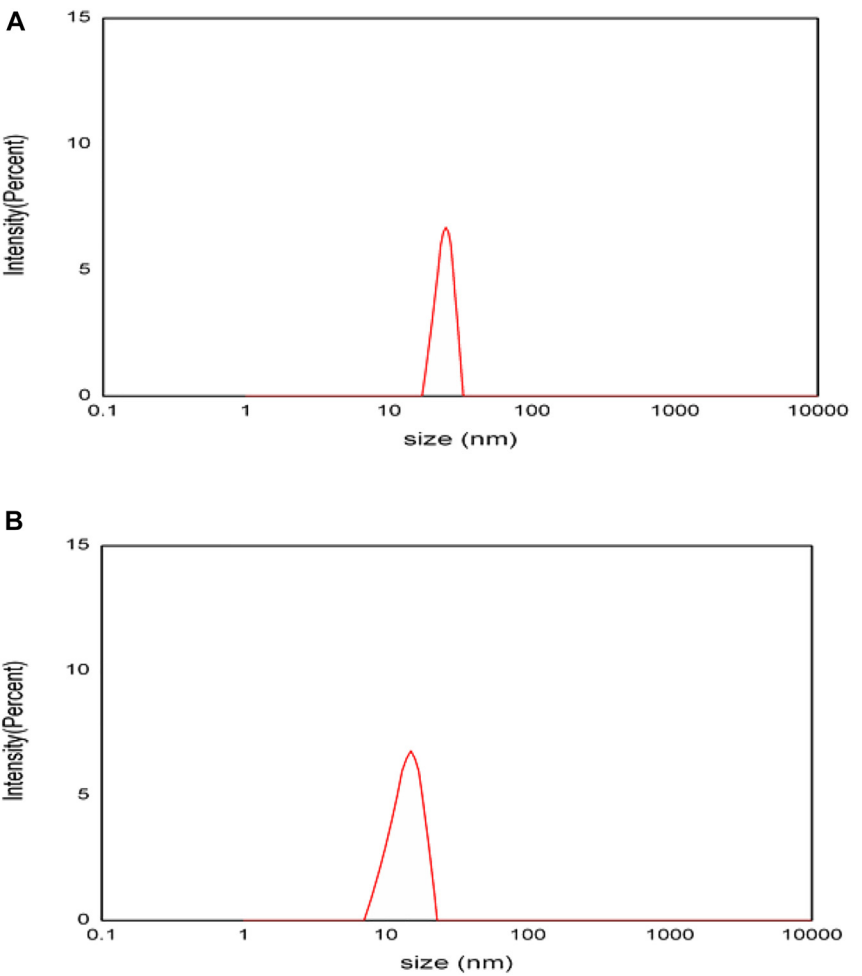

Figure 6: Particle size distribution of silver nanoparticles of sample A (modified BRUST method) and sample B (modified Turkevich method).

In the modified Turkevich method, $Na_3C_6H_5O_7.2H_2O$ and $C_6H_8O_6$ mixture solution was heated and then with continuous stirring added $AgNO_3$ solution. In this method, the impact of temperature and stirring rate was studied on the Zav of particles by maintaining the constant concentration of precursor and reducing agent. It can be seen in Table 2, by increasing the stirring from 400 to 1000 rpm caused a slight increase in Zav of AgNPs from 27 nm at 400 rpm to 30 nm at 1000 rpm. The increase in temperature from 60 °C to 75 °C reduced the size from 33 nm to 28 nm. The experimental conditions were optimized to synthesize smaller silver nanoparticles. The mixture solution of $Na_3C_6H_5O_7.2H_2O$ and $C_6H_8O_6$ was heated to 75 °C and magnetic stirring was carried out at 1400 rpm then 2 mL $AgNO_3$ (50 mM) solution was added immediately. Color change takes place from light yellow to reddish yellow. The synthesis of silver NPs can be verified by UV/vis analysis, which gives rise to characteristic peak between 380 and 450 nm. The samples were diluted enough to get absorbance within range. Several studies have shown that the absorption band from 200–800 is ideal for the characterization of silver nanoparticles in the sizes between 2 and 100 nm range [47]. The silver nanoparticles average (Zav) was measured by Zeta sizer and response are displayed in Tables 1 and 2. The results indicated that average size obtained by optimization of reaction conditions by modified BRUST method was 25 nm, while that of modified Turkevich method was 15 nm. The DLS technique operate on the principle of interaction of light with NPs. This technique is useful to determine the narrow size distribution NPs typically in the size range 2–500 nm [48]. The DLS technique is particularly more useful to analyses the particle size and size distribution in liquid suspensions or solutions [49], which could be utilized for different applications with tunned properties prepared using modified BRUST and Turkevich methods [31, 50–54], since these methods are eco-friendly versus other conventional techniques [13, 14, 55–57].

4 Conclusions

The silver nanoparticles were prepared by optimizing the conditions and properties were compared based on modified BRUST and Turkevich methods. The silver nanoparticles showed diameter in 15–25 range. Moreover, zeta potential values in case of BRUST and Turkevich methods was –31 mV and –36 mV, respectively. The particles shape was spherical and in dispersed form. The particles obtained by modified Turkevich method was more uniformly distributed. Results revealed that the silver nanoparticles size can be controlled following any method and by optimizing the synthesis conditions.

Acknowledgments: The authors express their gratitude to Princess Nourah bint Abdulrahman University Researchers Supporting Project (Grant No. PNURSP2022R11), Princess Nourah bint Abdulrahman University, Riyadh, Saudi Arabia.
Author contributions: All the authors have accepted responsibility for the entire content of this submitted manuscript and approved submission.
Research funding: This research was funded by Princess Nourah bint Abdulrahman University Researchers Supporting Project (Grant No. PNURSP2022R11), Princess Nourah bint Abdulrahman University, Riyadh, Saudi Arabia.
Conflict of interest statement: The authors declare no conflicts of interest regarding this article.

References

1. Shaheen M., Bhatti I. A., Ashar A., Mohsin M., Nisar J., Almoneef M. M., Iqbal M. Synthesis of Cu-doped MgO and its enhanced photocatalytic activity for the solar-driven degradation of disperse red F3BS with condition optimization. *Z. Phys. Chem.* 2021, *235*, 1395–1412.
2. Majid F., Shahin A., Ata S., Bibi I., Malik A., Ali A., Laref A., Iqbal M., Nazir A. The effect of temperature on the structural, dielectric and magnetic properties of cobalt ferrites synthesized via hydrothermal method. *Z. Phys. Chem.* 2021, *235*, 1279–1296.
3. Kamran U., Bhatti H. N., Iqbal M., Nazir A. Green synthesis of metal nanoparticles and their applications in different fields: a review. *Z. Phys. Chem.* 2019, *233*, 1325–1349.
4. Ghafoor A., Bibi I., Ata S., Majid F., Kamal S., Rehman F., Iqbal S., Aamir M., Slimani Y., Iqbal M. Synthesis and characterization of magnetically separable $La_{1-x}Bi_xCr_{1-y}Fe_yO_3$ and photocatalytic activity evaluation under visible light. *Z. Phys. Chem.* 2021, *235*, 1413–1431.
5. Noreen S., Ismail S., Ibrahim S. M., Kusuma H. S., Nazir A., Yaseen M., Khan M. I., Iqbal M. ZnO, CuO and Fe_2O_3 green synthesis for the adsorptive removal of direct golden yellow dye adsorption: kinetics, equilibrium and thermodynamics studies. *Z. Phys. Chem.* 2020, *235*, 1055–1075.
6. Bibi I., Hussain S., Majid F., Kamal S., Ata S., Sultan M., Din M. I., Iqbal M., Nazir A. Structural, dielectric and magnetic studies of perovskite $[Gd_{1-x}M_xCrO_3$ (M=La, Co, Bi)] nanoparticles: photocatalytic degradation of dyes. *Z. Phys. Chem.* 2019, *233*, 1431–1445.
7. Ata S., Tabassum A., Bibi I., Majid F., Sultan M., Ghafoor S., Bhatti M. A., Qureshi N., Iqbal M. Lead remediation using smart materials. A review. *Z. Phys. Chem.* 2019, *233*, 1377–1409.
8. Ata S., Tabassum A., Bibi I., Ghafoor S., Ahad A., Bhatti M. A., Islam A., Rizvi H., Iqbal M. Synthesis and characterization of ZnO nanorods as an adsorbent for Cr (VI) sequestration. *Z. Phys. Chem.* 2019, *233*, 995–1017.
9. Aljameel S. S., Almessiere M. A., Khan F. A., Taskhandi N., Slimani Y., Al-Saleh N. S., Manikandan A., Al-Suhaimi E. A., Baykal A. Synthesis, characterization, anti-cancer analysis of $Sr_{0.5}Ba_{0.5}Dy_xSm_xFe_{8-2x}O_{19}$ (0.00≤x≤1.0) microsphere nanocomposites. *Nanomaterials* 2021, *11*, 700.
10. Khan M., Mehmood B., Mustafa G. M., Humaiyoun K., Alwadai N., Almuqrin A. H., Albalawi H., Iqbal M. J. C. I. Effect of silver (Ag) ions irradiation on the structural, optical and photovoltaic

properties of Mn doped TiO_2 thin films based dye sensitized solar cells. *Ceram. Int.* 2021, *47*, 15801–15806.
11. Yasmin S., Nouren S., Bhatti H. N., Iqbal D. N., Iftikhar S., Majeed J., Mustafa R., Nisar N., Nisar J., Nazir A. Green synthesis, characterization and photocatalytic applications of silver nanoparticles using Diospyros lotus. *Green Process. Synth.* 2020, *9*, 87–96.
12. Ata S., Shaheen I., Qurat ul A., Ghafoor S., Sultan M., Majid F., Bibi I., Iqbal M. Graphene and silver decorated ZnO composite synthesis, characterization and photocatalytic activity evaluation. *Diam. Relat. Mater.* 2018, *90*, 26–31.
13. Awwad A. M., Salem N. M., Aqarbeh M. M., Abdulaziz F. M. Green synthesis, characterization of silver sulfide nanoparticles and antibacterial activity evaluation. *Chem. Int.* 2020, *6*, 42–48.
14. Remya V., Abitha V., Rajput P., Rane A., Dutta A. Silver nanoparticles green synthesis: a mini review. *Chem. Int.* 2017, *3*, 165–171.
15. Zhang W. S., Cao J. T., Dong Y. X., Wang H., Ma S. H., Liu Y. M. Enhanced chemiluminescence by Au-Ag core-shell nanoparticles: a general and practical biosensing platform for tumor marker detection. *J. Lumin.* 2018, *201*, 163–169.
16. Oh I.-h., Min H. S., Li L., Tran T. H., Lee Y.-k., Kwon I. C., Choi K., Kim K., Huh K. M. Cancer cell-specific photoactivity of pheophorbide a–glycol chitosan nanoparticles for photodynamic therapy in tumor-bearing mice. *Biomaterials* 2013, *34*, 6454–6463.
17. Hoshyar N., Gray S., Han H., Bao G. J. N. The effect of nanoparticle size on in vivo pharmacokinetics and cellular interaction. *Nanomedicine* 2016, *11*, 673–692.
18. Scott R. P., Quaggin S. E. The cell biology of renal filtration. *JCB (J. Cell Biol.)* 2015, *209*, 199–210.
19. Longmire M., Choyke P. L., Kobayashi H. Clearance properties of nano-sized particles and molecules as imaging agents: considerations and caveats. *Nanomedicine* 2008, *3*, 1–7.
20. Zhou Y., Dai Z. New strategies in the design of nanomedicines to oppose uptake by the mononuclear phagocyte system and enhance cancer therapeutic efficacy. *Chem. Asian J.* 2018, *3*, 3333–3340.
21. Chaloupka K., Malam Y., Seifalian A. M. Nanosilver as a new generation of nanoproduct in biomedical applications. *Trends Biotechnol.* 2010, *28*, 580–588.
22. Gliga A. R., Skoglund S., Wallinder I. O., Fadeel B., Karlsson H. L. Size-dependent cytotoxicity of silver nanoparticles in human lung cells: the role of cellular uptake, agglomeration and Ag release. *Part. Fibre Toxicol.* 2014, *11*, 1–17.
23. Liu D., Yu S., Zhu Z., Lyu C., Bai C., Ge H., Yang X., Pan W. Controlled delivery of carvedilol nanosuspension from osmotic pump capsule: in vitro and in vivo evaluation. *Int. J. Pharm.* 2014, *475*, 496–503.
24. Muhamad12 I. I., Selvakumaran S., Lazim N. A. M. Designing polymeric nanoparticles for targeted drug delivery system. *Nanomedicine* 2014, *287*, 287.
25. Muhammad Z., Raza A., Ghafoor S., Naeem A., Naz S. S., Riaz S., Ahmed W., Rana N. F. PEG capped methotrexate silver nanoparticles for efficient anticancer activity and biocompatibility. *Eur. J. Pharmaceut. Sci.* 2016, *91*, 251–255.
26. Wei L., Lu J., Xu H., Patel A., Chen Z.-S., Chen G. Silver nanoparticles: synthesis, properties, and therapeutic applications. *Drug Discov. Today* 2015, *20*, 595–601.
27. Almessiere M., Slimani Y., Algarou N., Gondal M., Wudil Y., Younas M., Auwal I., Baykal A., Manikandan A., Zubar T. Electronic, magnetic, and microwave properties of hard/soft nanocomposites based on hexaferrite $SrNi_{0.02}Zr_{0.02}Fe_{11.96}O_{19}$ with variable spinel phase MFe_2O_4 (M=Mn, Co, Cu, and Zn). *Ceram. Int.* 2021, *47*, 35209–35223.

28. Almessiere M. A., Slimani Y., Gungunes H., Manikandan A., Baykal A. Investigation of the effects of Tm^{3+} on the structural, microstructural, optical, and magnetic properties of Sr hexaferrites. *Results Phys.* 2019, *13*, 102166.
29. Slimani Y., Güngüneş H., Nawaz M., Manikandan A., El Sayed H. S., Almessiere M. A., Sözeri H., Shirsath S. E., Ercan I., Baykal A. Magneto-optical and microstructural properties of spinel cubic copper ferrites with Li-Al co-substitution. *Ceram. Int.* 2018, *44*, 14242–14250.
30. Slimani Y., Baykal A., Manikandan A. Effect of Cr^{3+} substitution on AC susceptibility of Ba hexaferrite nanoparticles. *J. Magn. Magn Mater.* 2018, *458*, 204–212.
31. Ali F., Hamza M., Iqbal M., Basha B., Alwadai N., Nazir A. State-of-art of silver and gold nanoparticles synthesis routes, characterization and applications: a review. *Z. Phys. Chem.* 2021, *236*, 291–326.
32. Dong X., Ji X., Wu H., Zhao L., Li J., Yang W. Shape control of silver nanoparticles by stepwise citrate reduction. *J. Phys. Chem. C* 2009, *113*, 6573–6576.
33. Zhang X.-F., Liu Z.-G., Shen W., Gurunathan S. Silver nanoparticles: synthesis, characterization, properties, applications, and therapeutic approaches. *Int. J. Mol. Sci.* 2016, *17*, 1534.
34. Das R., Nath S., Chakdar D., Gope G., Bhattacharjee R. Preparation of silver nanoparticles and their characterization. *J. Nanotechnol.* 2009, *5*, 1–6.
35. Taleb A., Petit C., Pileni M. P. Optical properties of self-assembled 2D and 3D superlattices of silver nanoparticles. *J. Phys. Chem. B* 1998, *102*, 2214–2220.
36. Link S., El-Sayed M. A. Optical properties and ultrafast dynamics of metallic nanocrystals. *Annu. Rev. Phys. Chem.* 2003, *54*, 331–366.
37. He R., Qian X., Yin J., Zhu Z. Preparation of polychrome silver nanoparticles in different solvents. *J. Mater. Chem.* 2002, *12*, 3783–3786.
38. Park J., Cha S.-H., Cho S., Park Y. Green synthesis of gold and silver nanoparticles using gallic acid: catalytic activity and conversion yield toward the 4-nitrophenol reduction reaction. *J. Nanoparticle Res.* 2016, *18*, 1–13.
39. Phongtongpasuk S., Poadang S., Yongvanich N. Environmental-friendly method for synthesis of silver nanoparticles from dragon fruit peel extract and their antibacterial activities. *Energy Proc.* 2016, *89*, 239–247.
40. Mandal A., Meda V., Zhang W., Farhan K., Gnanamani A. Synthesis, characterization and comparison of antimicrobial activity of PEG/TritonX-100 capped silver nanoparticles on collagen scaffold. *Colloids Surf. B Biointerfaces* 2012, *90*, 191–196.
41. Ban D. K., Paul S. Protein corona over silver nanoparticles triggers conformational change of proteins and drop in bactericidal potential of nanoparticles: polyethylene glycol capping as preventive strategy. *Colloids Surf. B Biointerfaces* 2016, *146*, 577–584.
42. Manno D., Filippo E., Di Giulio M., Serra A. Synthesis and characterization of starch-stabilized Ag nanostructures for sensors applications. *J. Non-Cryst. Solids* 2008, *354*, 5515–5520.
43. Šileikaitė A., Prosyčevas I., Puišo J., Juraitis A., Guobienė A. Analysis of silver nanoparticles produced by chemical reduction of silver salt solution. *Mater. Sci.* 2006, *12*, 1392–1320.
44. Rahimi-Nasrabadi M., Pourmortazavi S. M., Shandiz S. A. S., Ahmadi F., Batooli H. Green synthesis of silver nanoparticles using Eucalyptus leucoxylon leaves extract and evaluating the antioxidant activities of extract. *Nat. Prod. Res.* 2014, *28*, 1964–1969.
45. Hudlikar M., Joglekar S., Dhaygude M., Kodam K. Green synthesis of TiO_2 nanoparticles by using aqueous extract of Jatropha curcas L. latex. *Mater. Lett.* 2012, *75*, 196–199.
46. Dankovich T. A., Gray D. G. Bactericidal paper impregnated with silver nanoparticles for point-of-use water treatment. *Environ. Sci. Technol.* 2011, *45*, 1992–1998.

47. Fedlheim D. L., Foss C. A. *Metal Nanoparticles: Synthesis, Characterization, and Applications*; CRC Press: Boca Raton, USA, 2001; pp. 1–237.
48. Tomaszewska E., Soliwoda K., Kadziola K., Tkacz-Szczesna B., Celichowski G., Cichomski M., Szmaja W., Grobelny J. Detection limits of DLS and UV-Vis spectroscopy in characterization of polydisperse nanoparticles colloids. *J. Nanomater.* 2013, *2013*, 313081.
49. Murdock R. C., Braydich-Stolle L., Schrand A. M., Schlager J. J., Hussain S. M. Characterization of nanomaterial dispersion in solution prior to in vitro exposure using dynamic light scattering technique. *Toxicol. Sci.* 2008, *101*, 239–253.
50. Sasmaz M., Senel G. U., Obek E. Boron bioaccumulation by the dominant macrophytes grown in various discharge water environments. *Bull. Environ. Contam. Toxicol.* 2021, *106*, 1050–1058.
51. Sasmaz M., Senel G. U., Obek E. Strontium accumulation by the terrestrial and aquatic plants affected by mining and municipal wastewaters (Elazig, Turkey). *Environ. Geochem. Health* 2020, *43*, 1–14.
52. Sasmaz B., Sasmaz A., Hein J. R. Geochemical approach to the genesis of the Oligocene-stratiform manganese-oxide deposit, Chiatura (Georgia). *Ore Geol. Rev.* 2021, *128*, 103910.
53. Sasmaz A., Zagnitko V. M., Sasmaz B. Major, trace and rare earth element (REE) geochemistry of the Oligocene stratiform manganese oxide-hydroxide deposits in the Nikopol, Ukraine. *Ore Geol. Rev.* 2020, *126*, 103772.
54. Sasmaz A., Ozkan S., Gursu M. F., Sasmaz M. The hematological and biochemical changes in rats exposed to britholite mineral. *Appl. Radiat. Isot.* 2017, *129*, 185–188.
55. Shammout M. W., Awwad A. M. A novel route for the synthesis of copper oxide nanoparticles using Bougainvillea plant flowers extract and antifungal activity evaluation. *Chem. Int.* 2021, *7*, 71–78.
56. Amer M. W., Awwad A. M. Green synthesis of copper nanoparticles by Citrus limon fruits extract, characterization and antibacterial activity. *Chem. Int.* 2021, *7*, 1–8.
57. Al Banna L. S., Salem N. M., Jaleel G. A., Awwad A. M. Green synthesis of sulfur nanoparticles using Rosmarinus officinalis leaves extract and nematicidal activity against Meloidogyne javanica. *Chem. Int.* 2020, *6*, 137–143.